Activation and Propagation of Ca^{2+} Release during Excitation-Contraction Coupling in Atrial Myocytes

Jens Kockskämper, Katherine A. Sheehan, Dan J. Bare, Stephen L. Lipsius, Gregory A. Mignery, and Lothar A. Blatter

Department of Physiology, Stritch School of Medicine, Loyola University Chicago, Maywood, Illinois 60153, USA

ABSTRACT Fast two-dimensional confocal microscopy and the Ca^{2+} indicator fluo-4 were used to study excitation-contraction (E-C) coupling in cat atrial myocytes which lack transverse tubules and contain both subsarcolemmal junctional (j-SR) and central nonjunctional (nj-SR) sarcoplasmic reticulum. Action potentials elicited by field stimulation induced transient increases of intracellular Ca^{2+} concentration ($[Ca^{2+}]_i$) that were highly inhomogeneous. Increases started at distinct subsarcolemmal release sites spaced ~2 μm apart. The amplitude and the latency of Ca^{2+} release from these sites varied from beat to beat. Subsarcolemmal release fused to build a peripheral ring of elevated $[Ca^{2+}]_i$, which actively propagated to the center of the cells via Ca^{2+}-induced Ca^{2+} release. Resting myocytes exhibited spontaneous Ca^{2+} release events, including Ca^{2+} sparks and local (microscopic) or global (macroscopic) $[Ca^{2+}]_i$ waves. The microscopic $[Ca^{2+}]_i$ waves propagated in a saltatory fashion along the sarcolemma ("coupled" Ca^{2+} sparks) revealing the sequential activation of Ca^{2+} release sites of the j-SR. Moreover, during global $[Ca^{2+}]_i$ waves, Ca^{2+} release was evident from individual nj-SR sites. Ca^{2+} release sites were arranged in a regular three-dimensional grid as deduced from the functional data and shown by immunostaining of ryanodine receptor Ca^{2+} release channels. The longitudinal and transverse distances between individual Ca^{2+} release sites were both ~2 μm. Furthermore, electron microscopy revealed a continuous sarcotubular network and one peripheral coupling of j-SR with the sarcolemma per sarcomere. The results demonstrate directly that, in cat atrial myocytes, the action potential-induced whole-cell $[Ca^{2+}]_i$ transient is the spatio-temporal summation of Ca^{2+} release from subsarcolemmal and central sites. First, j-SR sites are activated in a stochastic fashion by the opening of voltage-dependent sarcolemmal Ca^{2+} channels. Subsequently, nj-SR sites are activated by Ca^{2+}-induced Ca^{2+} release propagating from the periphery.

INTRODUCTION

In mammalian cardiac myocytes, the action potential induces contraction of the cell by a process known as excitation-contraction (E-C) coupling. The transient increase of $[Ca^{2+}]_i$ underlying contraction is caused by Ca^{2+}-induced Ca^{2+} release (CICR) from the sarcoplasmic reticulum (SR), the major intracellular Ca^{2+} store. During CICR a small amount of Ca^{2+} influx through voltage-dependent L-type Ca^{2+} channels in the sarcolemma triggers the release of a much larger amount of Ca^{2+} from the SR via activation of Ca^{2+}-sensitive SR release channels, the ryanodine receptors (RyRs). In ventricular myocytes, the whole-cell $[Ca^{2+}]_i$ transient is thought to result from the spatio-temporal summation of individual localized Ca^{2+} release events or Ca^{2+} sparks (Cheng et al., 1993, 1996; Niggli, 1999; Wier and Balke, 1999). Ca^{2+} sparks are caused by the opening of a group of RyRs (Blatter et al., 1997). They originate from the junctional SR (j-SR) in the diadic cleft close to the T-tubules (Shacklock et al., 1995), where dihydropyridine receptor (DHPR) L-type Ca^{2+} channels and RyRs are colocalized (Lewis Carl et al., 1995; Scriven et al., 2000). Because an extensive T-tubular network conducts the action potential deep into the cell (Soeller and Cannell, 1999), Ca^{2+} release takes place virtually simultaneously throughout the ventricular myocyte. Thus, the $[Ca^{2+}]_i$ increase seems uniform rather than composed of discrete events (Cheng et al., 1994). Reduction of the T-tubular network in ventricular myocytes leads to spatial inhomogeneities of the $[Ca^{2+}]_i$ transient (Lipp et al., 1996), underlining the importance of this membrane system for ventricular E-C coupling. Ca^{2+} release from individual sites, however, can be visualized (1) when Ca^{2+} influx through L-type channels is manipulated (Cannell et al., 1994; Lopez-Lopez et al., 1994; Santana et al., 1996); (2) when the diffusion distance of free $[Ca^{2+}]_i$ is reduced (Cleemann et al., 1998; Song et al., 1998); or (3) when ultrafast linescan imaging is used (Tanaka et al., 1998).

Because Ca^{2+} sparks also are observed in atrial myocytes (Blatter et al., 1997; Hüser et al., 1996), it seems straightforward to assume that the atrial $[Ca^{2+}]_i$ transient is likewise the result of the spatial and temporal summation of such elementary SR Ca^{2+} release events. However, no direct evidence for this hypothesis has been obtained so far. Moreover, the ultrastructure of atrial myocytes, especially with respect to the key membranes and proteins involved in the E-C coupling process, differs substantially from ventricular myocytes. In particular, the absence of a T-tubular system in atrial (and Purkinje) myocytes (Cordeiro et al., 2001; Hüser et al., 1996;

Received for publication 20 April and in final form 20 July 2001.

Address reprint requests to Lothar A. Blatter, Department of Physiology, Stritch School of Medicine, Loyola University Chicago, 2160 South First Avenue, Maywood, IL 60153. Tel.: 708-216-1182; Fax: 708-216-6308; E-mail: lblatte@lumc.edu.

0006-3495/01/11/2590/16 $2.00

McNutt and Fawcett, 1969) divides the SR into j-SR and nj-SR compartments and has been shown to result in spatially and temporally inhomogeneous $[Ca^{2+}]_i$ transients (Berlin, 1995; Cordeiro et al., 2001; Hatem et al., 1997; Hüser et al., 1996, 2000; Lipp et al., 1990; Mackenzie et al., 2001; Pott et al., 1991). Thus, to understand atrial E-C coupling it is important to determine the subcellular distribution and the participation of individual Ca^{2+} release sites as well as the specific roles which j-SR and nj-SR play in this process.

To address these issues, we used one- and two-dimensional (2-D) confocal microscopy in combination with a fluorescent Ca^{2+} indicator to visualize Ca^{2+} release from subsarcolemmal j-SR and central nj-SR in isolated cat atrial myocytes during action potential-induced $[Ca^{2+}]_i$ transients. In addition, spontaneously occurring Ca^{2+} sparks and waves were used as a tool to identify the location and activation of individual SR Ca^{2+} release sites. Using immunocytochemistry and electron microscopy we also determined the subcellular distribution of RyRs and SR, respectively. Taken together, the results demonstrate that in cat atrial myocytes, the whole-cell $[Ca^{2+}]_i$ transient results from the spatio-temporal summation of Ca^{2+} released from individual sites in the subsarcolemmal j-SR and the central nj-SR. The variable latency and magnitude of Ca^{2+} release from the subsarcolemmal sites suggest that it is triggered by stochastic openings of L-type Ca^{2+} channels. Central release sites, in contrast, are activated by CICR propagating from the j-SR.

MATERIALS AND METHODS

Preparation of cells

The procedure used for the isolation of atrial myocytes from the cat heart was in accordance with local and national guidelines for animal care. It has been described in detail previously (Wu et al., 1991). Briefly, cats of either sex were anesthetized with thiopental sodium (35 mg kg^{-1} intraperitoneally). After thoracotomy hearts were quickly excised, mounted on a Langendorff apparatus, and retrogradely perfused with collagenase-containing solution at 37°C.

Freshly isolated myocytes were plated on glass coverslips and loaded with the Ca^{2+}-sensitive fluorescent dye fluo-4 (Molecular Probes, Eugene, OR) by 20–40 min exposure to Tyrode solution (in mM: 140 NaCl, 5 KCl, 2 $CaCl_2$, 1 $MgCl_2$, 10 glucose, and 10 HEPES; pH 7.35 with NaOH) containing 20–45 μM of the acetoxymethyl ester of the dye (dissolved in 20% (w/v) Pluronic F-127/dimethyl sulfoxide; Molecular Probes). At least 15 min were allowed for de-esterification of the indicator.

Electrical stimulation

$[Ca^{2+}]_i$ transients were evoked by 2–4 ms suprathreshold rectangular voltage pulses through a pair of extracellular platinum electrodes. Cells were paced at 0.5–0.7 Hz. All experiments were performed at room temperature (22–24°C).

Drugs

Ryanodine (Calbiochem, La Jolla, CA) and thapsigargin (Alexis, San Diego, CA) were used to disable the sarcoplasmic reticulum. Stock solutions were prepared in either ethanol (5 mM ryanodine) or dimethyl sulfoxide (10 mM thapsigargin) and diluted in the Tyrode solution to give final concentrations of 10 μM ryanodine and 2 μM thapsigargin.

2-D confocal Ca^{2+} imaging

A glass coverslip with dye-loaded myocytes was transferred to the stage of an inverted microscope (Nikon Diaphot 300, Fryer Company Inc., Huntley, IL). For 2-D confocal Ca^{2+} imaging a Nipkow dual-disc type laser scanning unit (CSU10, Yokogawa Electric Co., Tokyo, Japan; Genka et al., 1999) was used. The scanning unit consisted of two spatially separated but mechanically connected discs, a microlens disc and a pinhole disc. Light (488 nm) from an attached argon ion laser (532-A-A04, Omnichrome, Chino, CA) was focused through the microlenses to the corresponding pinholes (diameter, 50 μm) and through the objective lens (Nikon CF Plan Apochromat, water, ×60, n.a. = 1.2) on a plane in the specimen. The emitted fluorescence (>515 nm) was collected by an intensified charge-coupled device camera (Stanford Photonics, Palo Alto, CA). Images (512 pixels × 480 pixels, 8-bit resolution, interlaced) were acquired at video rate (30 Hz) and stored on a real-time disc for later analysis. After background subtraction normalized fluorescence (F/F_0) images were calculated. The F_0 image was created by averaging the five images immediately preceding the event(s) of interest. F/F_0 images were de-interlaced resulting in a temporal resolution of 60 Hz. The spatial (x-y) resolution of these ratio images was 0.33 μm × 0.54 μm. Areas of interest of 0.71 μm^2 were chosen for the analysis of subcellular $[Ca^{2+}]_i$ signals. Changes of $[Ca^{2+}]_i$ are expressed as changes of F/F_0.

Linescan imaging

Fast, 1-D (linescan) imaging was performed using a confocal laser scanning unit (LSM 410, Carl Zeiss, Jena,Germany) attached to an inverted microscope (Axiovert 100, Zeiss) with a ×40 oil-immersion objective lens (Plan-Neofluar, n.a. = 1.3, Zeiss). Fluo-4 was excited with the 488 nm line of the argon ion laser and the emitted fluorescence was collected at >515 nm. For linescan imaging (8-bit), the specimen was scanned repetitively at 1.4 ms or 2.1 ms intervals. Linescan images (8-bit) are presented as background-subtracted F/F_0 images.

Immunocytochemistry

Acutely isolated atrial myocytes were seeded onto poly-D-lysine coated glass coverslips. After attachment the cells were washed in buffer A (450 mM NaCl, 20 mM phosphate buffer, pH 7.2) and then fixed for 30 min with 4% (w/v) paraformaldehyde in 200 mM phosphate buffer (pH 7.4), followed by washing with buffer A. The cells were permeabilized with buffer B (0.3% Triton X-100, 450 mM NaCl, 20 mM phosphate buffer, pH 7.2) containing 1% goat serum. Cells were subjected to immunocytochemical analysis using antibodies directed against α-actinin and RyRs. Both primary antibodies used were mouse-derived monoclonals. Anti-α-actinin antibody (IgG_1; clone EA-53; Sigma, St. Louis, MO) was used at a dilution of 1:250 and the anti-RyR antibody (IgG_1; clone 34-C; Affinity Bioreagents Inc., Golden, CO) at 1:50. The myocytes were incubated for at least 45 min in buffer B containing 10% goat serum and primary antibody directed against either α-actinin or RyR. After washing in buffer A, the cells were then incubated for 30 min with secondary antibody (dilution 1:400), Alexa Fluor 594-conjugated goat anti-mouse IgG (Molecular Probes). RyR and α-actinin immunoreactivity was visualized by confocal microscopy. The fluorophore was excited with the 514-nm line of the argon ion laser (LSM 410, Zeiss) or with the 543-nm line of the green HeNe laser

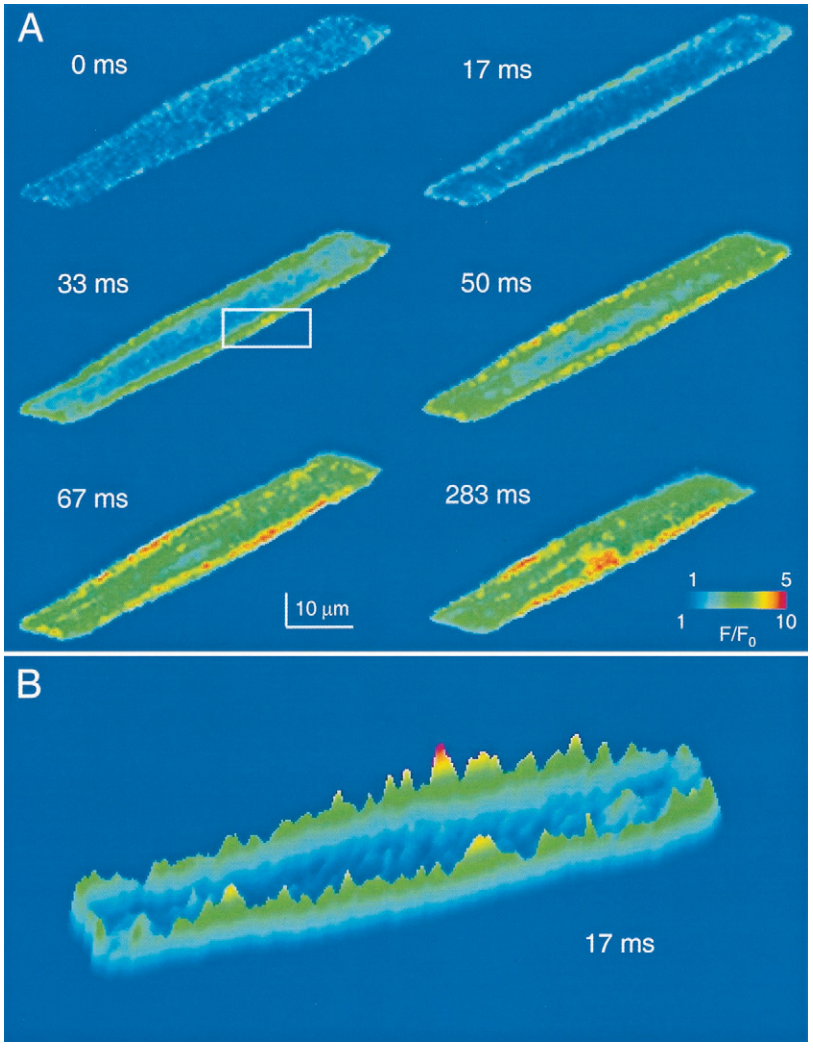

FIGURE 1 Characteristics of the atrial action potential-induced $[Ca^{2+}]_i$ transient as visualized by 2-D confocal microscopy. (*A*) Series of color-coded F/F_0 images. $[Ca^{2+}]_i$ starts to rise in the subsarcolemmal space. A ring of elevated $[Ca^{2+}]_i$ develops and propagates to the center of the cell. Boxed area (33 ms) is shown in detail in Fig. 2 *Aa*. The F/F_0 scale from 1 to 5 refers to the first image (0 ms) only. (*B*) The surface plot view of the image recorded at 17 ms (panel *A*) reveals distinct $[Ca^{2+}]_i$ peaks in the subsarcolemmal space at the beginning of the $[Ca^{2+}]_i$ transient.

(Radiance 2000 MP, Bio-Rad, Hercules, CA). Fluorescence was recorded at >600 nm. In some experiments, transmitted light images were acquired simultaneously with a photodiode detector.

Transmission electron microscopy

Isolated atrial myocytes were placed on Pioloform-coated Aclar embedding film (Ted Pella Inc., Redding, CA) and allowed to settle for 2 h, assuring adequate adherence for subsequent processing. Fixation with 4% glutaraldehyde (Electron Microscopy Sciences, Ft. Washington, PA) was followed by a 0.1 M cacodylate buffer wash and post staining with 1% osmium tetroxide (Electron Microscopy Sciences). Myocytes were serially dehydrated in ethanol and infiltrated with EM bed-812 epoxy resin (Electron Microscopy Sciences). Final embedding entailed inverting a previously polymerized resin block over preselected areas at 56°C for 24 h. The Aclar film was peeled away from the blocks leaving the cells exposed for immediate en face thin sectioning on a diamond knife at 80 nm. Sections were picked up on copper grids and counterstained with 5% uranyl acetate and Reynolds' lead citrate (Reynolds, 1963). Grids were examined and photographed on a Hitachi H-600 transmission electron microscope (Tokyo, Japan) at 75 kV.

Data

Where appropriate, data are presented as mean ± S.E. For the measurements of distances between SR Ca^{2+} release sites *n* refers to the number of distances averaged between the indicated number of release sites analyzed.

RESULTS

2-D imaging of the atrial $[Ca^{2+}]_i$ transient

The characteristic 2-D features of atrial action potential-induced $[Ca^{2+}]_i$ transients (n >50) are illustrated in Fig. 1. A single cat atrial myocyte was stimulated at 0.5 Hz. Fig. 1

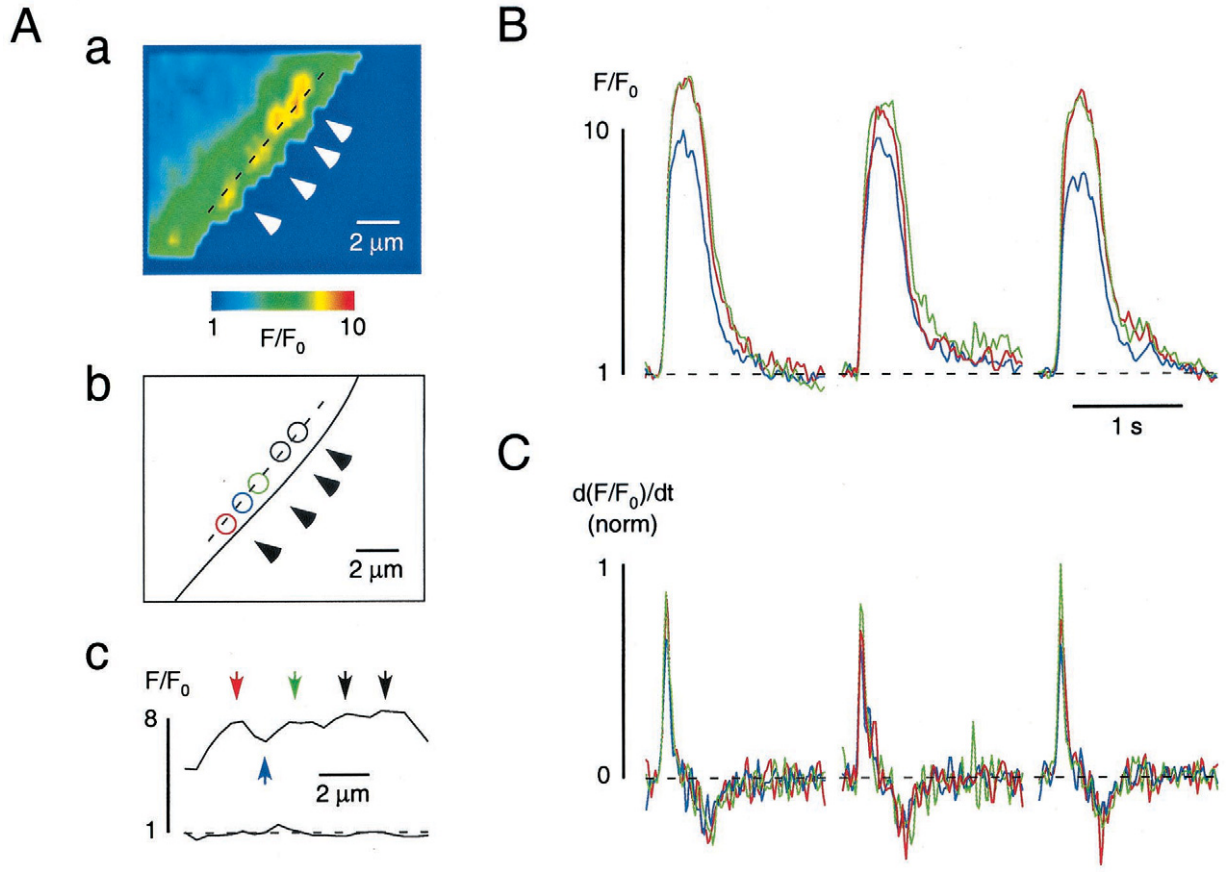

FIGURE 2 Identification of individual Ca^{2+} release sites of the subsarcolemmal j-SR. (*A*) Enlarged view (*a*) of the boxed area in Fig. 1 *A* (33 ms) shows four neighboring sites of higher $[Ca^{2+}]_i$ (*arrowheads*) in the cell periphery as schematically depicted in (*b*). (*c*) Fluorescence profile along the dashed line in (*a*). Release sites (*black*, *green*, and *red circles* and *arrows*) have higher amplitude $[Ca^{2+}]_i$ transients (*B*) and higher approximated Ca^{2+} release fluxes (*C*) than a nonrelease site (*blue circle* and *arrow*) located between the red and green release sites. Stimulation frequency, 0.5 Hz.

A shows a series of color-coded, 2-D images of the resulting $[Ca^{2+}]_i$ transient at a central axial depth of the cell. The images show the myocyte immediately after depolarization ($t = 0$ ms), during the subsequent initial rising phase of the $[Ca^{2+}]_i$ transient (17–67 ms), and during maximal contraction (283 ms). Electrical stimulation of the cell resulted in an increase in $[Ca^{2+}]_i$ that started at discrete spots along the periphery (17 ms) as shown in detail in the surface plot in Fig. 1 *B*. These sites subsequently fused to form a subsarcolemmal "ring" of elevated $[Ca^{2+}]_i$ (33 ms) that propagated to the cell center. Marked non-uniformities of the $[Ca^{2+}]_i$ signal were observed during this process both in the periphery and in the center of the cell. Fig. 2 reveals details about the inhomogeneities found in the subsarcolemmal region. Fig. 2 *Aa* shows an enlarged view of the boxed area of the cell depicted in Fig. 1 *A* (33 ms). At least four sites of elevated $[Ca^{2+}]_i$ (marked by the *white arrowheads*) are clearly visible. They were located directly underneath the plasma membrane and spaced ~2 μm apart as confirmed by the profile plot along the dashed line (Fig. 2 *Ac*). The $[Ca^{2+}]_i$ signals originating from two of these sites (*red* and *green circles* in Fig. 2 *Ab*) and from a region in between (*blue circle*) were analyzed for three consecutive transients. Their amplitude and the first derivative of their amplitude, which gives a good approximation of the underlying SR Ca^{2+} release flux (Sipido and Wier, 1991; Song et al., 1998), are shown in Fig. 2, *B* and *C*, respectively. Although both parameters varied slightly from beat to beat, $[Ca^{2+}]_i$ transient amplitude and peak release flux were always higher at the red and green sites than at the blue site. Thus, a persistent local $[Ca^{2+}]_i$ gradient was observed between both the red and green sites and the blue site, an observation that would have escaped conventional transverse linescan imaging. This gradient in conjunction with the higher underlying Ca^{2+} release flux suggests that the red and green sites represent subsarcolemmal Ca^{2+} release sites from the j-SR, whereas the blue site is a nonrelease site. Similar results were obtained in five atrial myocytes. The subsarcolemmal sites chosen for analysis were located in central parts of the myocyte in which cell movement during action potential-induced contractions is negligible. Nonetheless, despite cell motion very similar patterns of putative Ca^{2+}

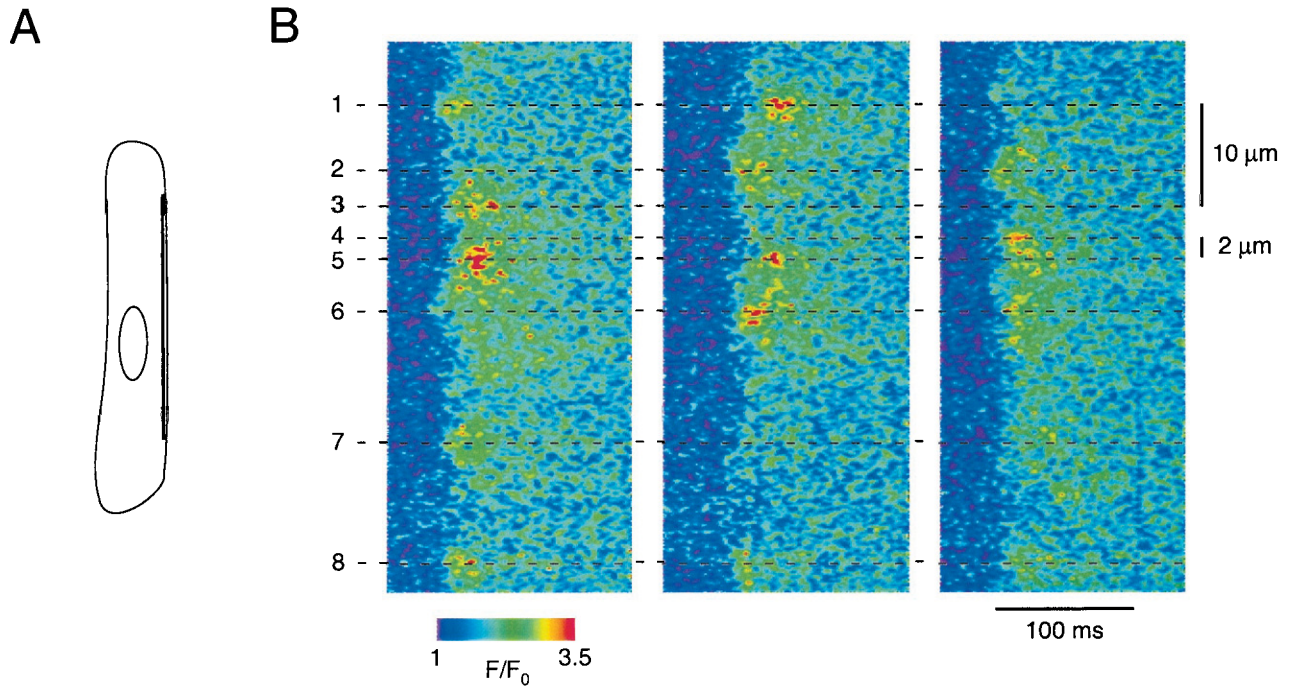

FIGURE 3 Ca^{2+} release from subsarcolemmal release sites has variable amplitudes and latencies. (*A*) Position of the scanned line. (*B*) Linescan images of three consecutive $[Ca^{2+}]_i$ transients. Eight release sites are identified along the dashed lines. Their location is constant, but their amplitudes and activation order vary from beat to beat. Stimulation frequency, 0.7 Hz.

release sites were also observed at the cell ends. However, such sites were not included in the analysis. Furthermore, no motion was detected during the initial 50 ms of the $[Ca^{2+}]_i$ transient, i.e., at a time when individual release sites became detectable.

For a more detailed kinetic analysis of the $[Ca^{2+}]_i$ signals originating from the j-SR release sites, additional experiments were performed in the linescan mode of a conventional laser scanning confocal microscope (Zeiss LSM 410) with an increased temporal resolution (1.4 ms per line). The scanned line was positioned parallel to the longitudinal axis of the cell directly underneath the sarcolemma as depicted in Fig. 3 *A*. The myocyte was stimulated at 0.7 Hz and three consecutive subsarcolemmal $[Ca^{2+}]_i$ transients were compared (Fig. 3 *B*). Release sites were identified as regions of high fluorescence as compared with neighboring sites of low fluorescence. Release occurred at eight specific locations that were constant during repetitive stimulations as indicated by the dashed lines in Fig. 3 *B*. The distance between individual release sites was ~2 μm (e.g., sites 4 and 5) or a multiple thereof (e.g., sites 1 and 3) confirming the results obtained by 2-D imaging (Fig. 2). At higher time resolution, however, a beat-to-beat variability in the activation order of individual release sites and in the amplitude of the local $[Ca^{2+}]_i$ transients was evident. For example, site 1 activated early in the first transient, but much later and with a higher amplitude during the second transient, and barely detectable in the third one, thus revealing beat-to-beat alterations of latency of activation. Sites 3, 5, and 7 displayed a high amplitude signal during the first $[Ca^{2+}]_i$ transient and then showed less release in the later transients. By contrast, sites 2, 4, and 6 revealed low $[Ca^{2+}]_i$ levels during the first transient but were clearly activated during the second and/or third transient. Finally, for site 8, both the latency and the amplitude of Ca^{2+} release were fairly constant during the three beats. Similar observations were made in six cells. In three of these cells, 34 subsarcolemmal release sites were identified with a mean distance of 1.90 ± 0.04 μm ($n = 31$).

Taken together, the results demonstrate that Ca^{2+} release from j-SR occurs at specific locations spaced ~2 μm apart. The location of the release sites was stable during consecutive stimulations. However, their activation order and the amount of Ca^{2+} released from an individual site varied significantly from beat to beat.

The inward spread of the $[Ca^{2+}]_i$ transient

Fig. 4 illustrates the spatio-temporal inhomogeneities in $[Ca^{2+}]_i$ observed during the inward spread of the action potential-induced $[Ca^{2+}]_i$ transient in an atrial myocyte. The images in Fig. 4 *A* were obtained 33 ms (*Aa*), 67 ms (*Ab*), and 100 ms (*Ac*) after the beginning of the $[Ca^{2+}]_i$ transient. After the development of the ring of elevated $[Ca^{2+}]_i$ (*Aa*), three punctate rows of higher $[Ca^{2+}]_i$ (*Ab–Ac*; marked by *arrows*) became visible inside the cell. These rows were

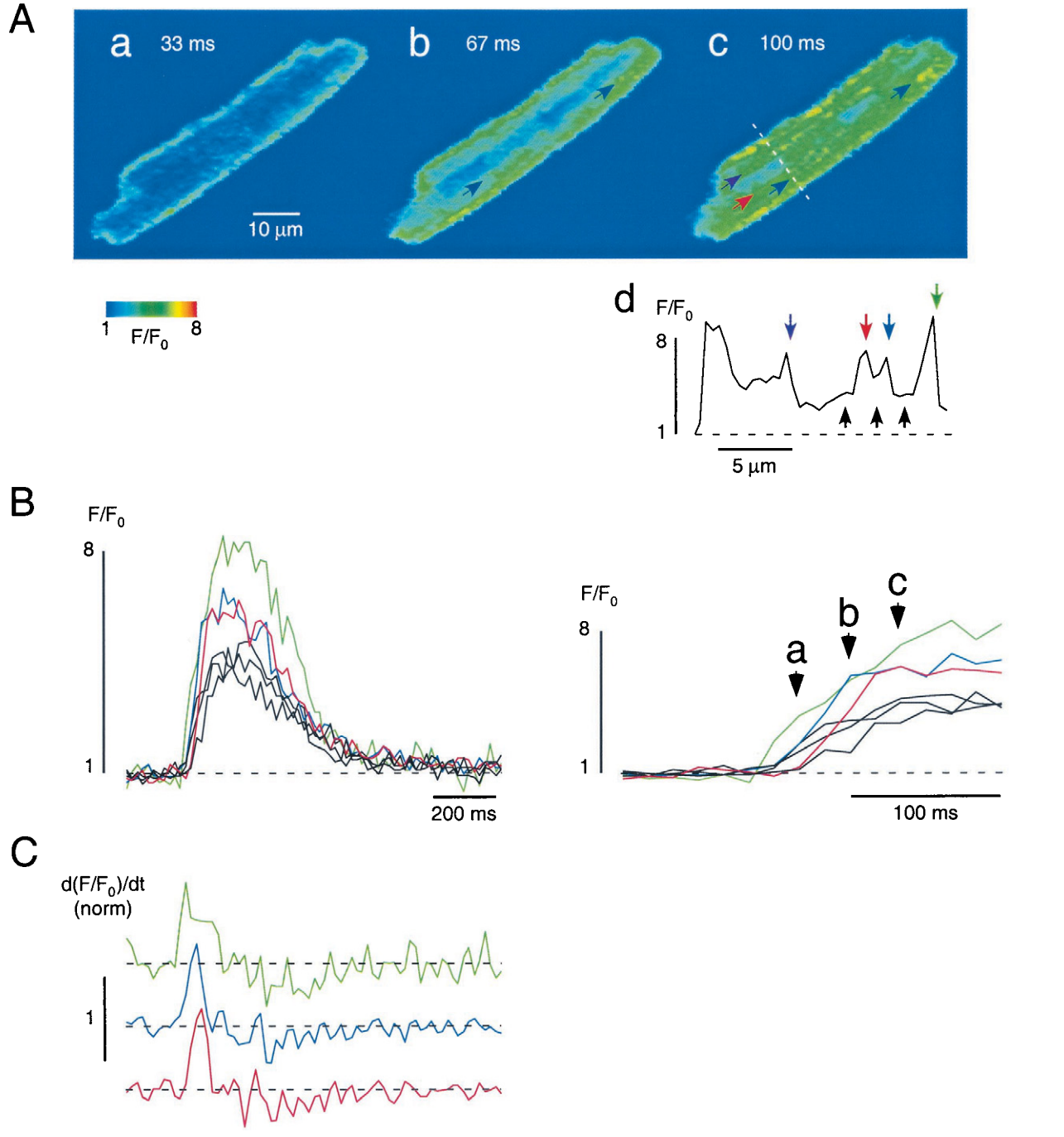

FIGURE 4 The atrial $[Ca^{2+}]_i$ transient spreads inwardly via propagating CICR. (*A*) 2-D images (*a–c*) of an atrial myocyte during an action potential-induced $[Ca^{2+}]_i$ transient. Punctate rows of higher $[Ca^{2+}]_i$ develop during the transient. They are marked by the arrows. (*d*) Fluorescence profile along the dashed line in (*c*). Sites of higher (*colored arrows*) and lower (*black arrows*) $[Ca^{2+}]_i$ can be distinguished. (*B*) $[Ca^{2+}]_i$ transients of the sites marked by the arrows in (*Ad*). The beginning of the transients is shown on an expanded time scale on the right. Labels *a*, *b*, and *c* refer to the images in (*A*). (*C*) Normalized approximated Ca^{2+} release fluxes of the three colored release sites shown in (*Ad*). Release flux peaks consecutively from the periphery (*green trace*) to the center (*red trace*) of the cell, indicating that CICR propagates from the subsarcolemmal j-SR to the central nj-SR.

approximately parallel to the longitudinal axis of the myocyte and separated by ~2–4 μm as confirmed by the profile plot (Fig. 4 *Ad*) along the dashed line in Fig. 4 *Ac*.

In Fig. 4 *B* (*left panel*), local $[Ca^{2+}]_i$ transients originating from the sites of elevated $[Ca^{2+}]_i$ (*green*, *blue*, and *red arrows* in Fig. 4 *Ad*) were compared with those sites exhibiting low $[Ca^{2+}]_i$ (*black arrows* in Fig. 4 *Ad*). The colored sites displayed large amplitude $[Ca^{2+}]_i$ transients with high rates of rise, indicating Ca^{2+} release sites from the subsarcolemmal j-SR (*green*) and the central nj-SR (*blue* and *red*).

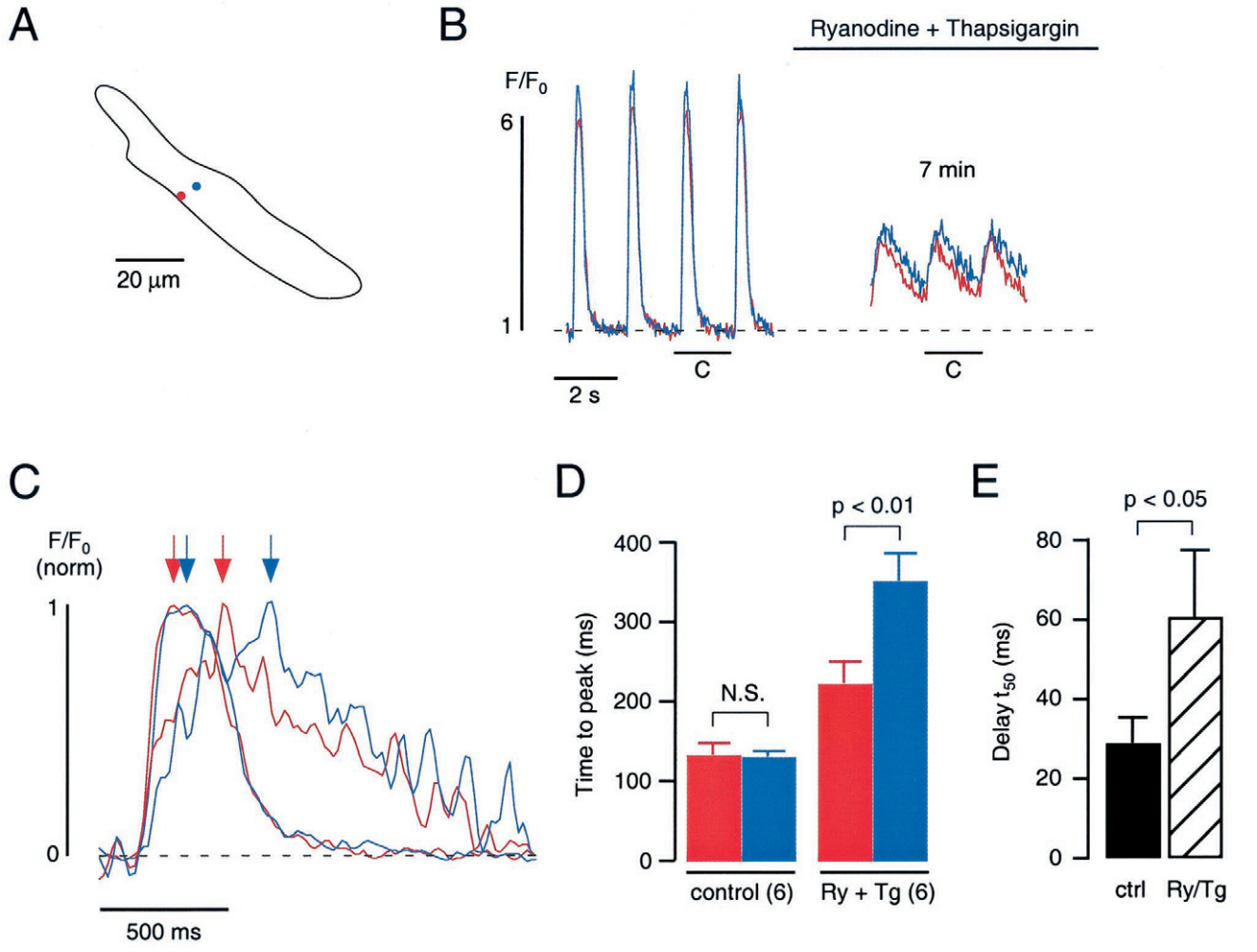

FIGURE 5 Disabling SR function slows down the centripetal spread of Ca^{2+}. (*A*) Atrial myocyte and subcellular regions (~1 μm^2) studied. (*B*) Local $[Ca^{2+}]_i$ transients of the regions shown in *A* before and after inhibition of SR function by 10 μM ryanodine and 2 μM thapsigargin. Blockade of the SR increases diastolic $[Ca^{2+}]_i$, decreases the amplitude, and slows down the kinetics of the $[Ca^{2+}]_i$ transients. (*C*) Normalized $[Ca^{2+}]_i$ transients from *B*. Arrows indicate the maximum amplitudes. Under control conditions (*smooth traces*) the subsarcolemmal $[Ca^{2+}]_i$ transient (*red*) slightly precedes the central $[Ca^{2+}]_i$ transient (*blue*); however, both have similar time courses. After inhibition of the SR (*noisy traces*), the kinetics of both $[Ca^{2+}]_i$ transients are slowed down. Importantly, the central $[Ca^{2+}]_i$ transient is delayed significantly, indicating that the spread of Ca^{2+} from the periphery to the center is slower under these conditions. (*D*) Rise times (times to peak) of subsarcolemmal (*red*) and central (*blue*) $[Ca^{2+}]_i$ transients before (control) and after (Ry + Tg) inhibition of SR function. (*E*) Delay between the half-maximum $[Ca^{2+}]_i$ transient amplitudes (delay t_{50}) of subsarcolemmal and central sites before (ctrl) and after (Ry/Tg) blockade of the SR. Mean data from six myocytes. N.S., not statistically significant. Stimulation frequency, 0.6 Hz.

By contrast, the sites represented by the black traces had much smaller amplitude $[Ca^{2+}]_i$ transients with low rates of rise, defining them as nonrelease sites. Fig. 4 *B* also demonstrates that the maximum $[Ca^{2+}]_i$ transient amplitude was higher at the subsarcolemmal site than at the central sites. This was a consistent finding. In a total of 10 atrial myocytes, the $[Ca^{2+}]_i$ transient amplitude of the central release sites reached only 76.4 ± 4.1% (n = 10) of that recorded from neighboring subsarcolemmal sites. The right panel in Fig. 4 *B* shows the beginning of the local $[Ca^{2+}]_i$ transients on an expanded time scale (*a*, *b*, and *c* refer to the images in Fig. 4 *A*). Marked differences in the onset of the transients are obvious. $[Ca^{2+}]_i$ started to rise first at the subsarcolemmal release site (*green trace*). With a delay of 17 ms and 33 ms, the $[Ca^{2+}]_i$ increase became evident at the more central release sites (*blue* and *red traces*, respectively). Accordingly, the approximated release fluxes of the central sites reached their maximum 33 ms and 50 ms after the subsarcolemmal site (Fig. 4 *C*; colors as before). Thus, Ca^{2+} release sites were recruited consecutively from the periphery to the center of the cell by propagating CICR. If this conclusion is correct, inhibition of SR function should slow down the centripetal spread of Ca^{2+}. To test this hypothesis additional experiments were performed in the absence and presence of ryanodine and thapsigargin to abolish SR function.

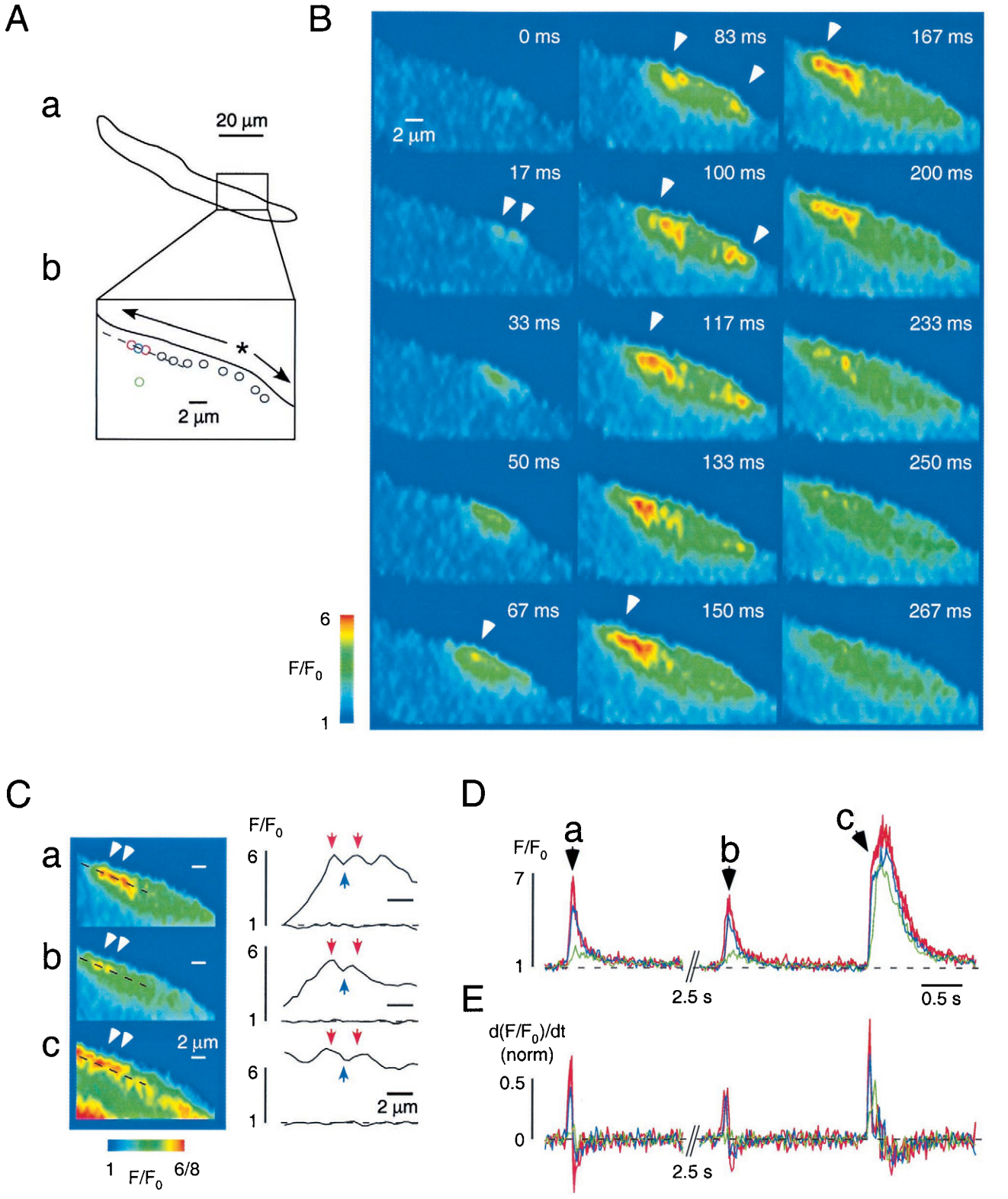

FIGURE 6 Microscopic $[Ca^{2+}]_i$ waves ("coupled" Ca^{2+} sparks) reveal the location of individual Ca^{2+} release sites from the subsarcolemmal j-SR. (*A*) Atrial myocyte (*a*) and subcellular region (*b*) where the microscopic wave shown in *B* occurred. Black and red circles indicate the subsarcolemmal Ca^{2+} release sites. The green circle indicates a central site and the blue circle marks a nonrelease site. $[Ca^{2+}]_i$ signals of the colored sites are plotted in *D* and *E*. Asterisk and arrows indicate wave origin and wave spread, respectively. (*B*) Sequential images of a microscopic $[Ca^{2+}]_i$ wave. Individual Ca^{2+} release sites are visible as discrete spots of higher $[Ca^{2+}]_i$. Their first appearance is marked by the arrowheads. The wave starts at two sites (17 ms) and propagates along the sarcolemma in both directions. (*C*) Snapshots taken at three different times: (*a*) during the wave shown in *B*, (*b*) during a second wave, and (*c*)

Fig. 5 *B* shows $[Ca^{2+}]_i$ transients originating from a subsarcolemmal (red) and a neighboring central region (blue) of an atrial myocyte (Fig. 5 *A*). Inhibition of SR function by ryanodine and thapsigargin increased diastolic $[Ca^{2+}]_i$ levels and markedly decreased the $[Ca^{2+}]_i$ transient amplitudes both in the periphery and the center of the cell. Furthermore, it slowed down the kinetics of the $[Ca^{2+}]_i$ transients. This is shown in more detail in Fig. 5 *C*. $[Ca^{2+}]_i$ transients recorded before (*smooth traces*) and after inhibition of the SR (*noisy traces*) are plotted on an expanded time scale. For better comparison their amplitudes have been normalized. In the presence of a functional SR, the central signal follows the subsarcolemmal $[Ca^{2+}]_i$ transient with a short delay. When the SR was disabled, however, both transients were considerably slower and the delay between the central and subsarcolemmal signal was greatly increased. To quantify the time course of Ca^{2+} movement from the periphery to the center of the cells, we determined the delay between the half-maximum amplitudes of the subsarcolemmal and central $[Ca^{2+}]_i$ transients (delay t_{50}), and we measured the rise times of the $[Ca^{2+}]_i$ transients. Mean data from six myocytes are presented in Fig. 5, *D* and *E*. Under control conditions rise times for subsarcolemmal and central $[Ca^{2+}]_i$ transients were almost identical with times to peak of ~130 ms (Fig. 5 *D*; $n = 6$). The delay between their half-maximum amplitudes was 28 ± 7 ms (Fig. 5 *E*; $n = 6$). After inhibition of the SR, rise times for both the peripheral and central signals were significantly prolonged to 220 ± 30 ms and 349 ± 39 ms, respectively (Fig. 5 *D*; $n = 6$, $p < 0.01$). In addition, the delay between their half-maximum amplitudes was doubled to 60 ± 17 ms (Fig. 5 *E*; $n = 6$, $P < 0.05$ vs. control). Collectively, these data confirm that the spread of Ca^{2+} from the periphery to the center of the cells is an active process involving propagating CICR.

Activation of individual Ca^{2+} release sites from the j-SR during microscopic $[Ca^{2+}]_i$ waves

In resting myocytes two kinds of spontaneous Ca^{2+} release events were observed, i.e., Ca^{2+} sparks and $[Ca^{2+}]_i$ waves. Ca^{2+} sparks occurred both in the subsarcolemmal and, less frequently, in the central regions confirming previous results obtained in these cells (Hüser et al., 1996). Furthermore, two different types of $[Ca^{2+}]_i$ waves were found: (1) macroscopic (global) waves that traveled through the entire cell and (2) microscopic (local) waves that propagated in a saltatory fashion over several micrometers along the periphery of the myocyte. Microscopic $[Ca^{2+}]_i$ waves had the appearance of "coupled" Ca^{2+} sparks and did not cause any measurable contraction. By contrast, macroscopic waves led to substantial contractions comparable with those observed during action potential-induced $[Ca^{2+}]_i$ transients.

Fig. 6 *B* shows a sequence of images illustrating the development and propagation of a microscopic $[Ca^{2+}]_i$ wave. The subcellular region shown corresponds to the box in Fig. 6 *A*. Ten individual release sites were identified during this wave as depicted in Fig. 6 *Ab* (*red* and *black circles*). The wave started at two distinct sites marked by the arrowheads in Fig. 6 *B* (17 ms) and the asterisk in Fig. 6 *Ab*. It then propagated with an average velocity of ~100 $\mu m\ s^{-1}$ over six more sites to the left, starting at 67 ms, and over two more sites to the right, starting at 83 ms. The individual SR release sites were identified as distinct $[Ca^{2+}]_i$ peaks clearly visible in most of the images. Their first appearance is indicated by the arrowheads. The sites were located close to the edge of the cell suggesting that the Ca^{2+} release originated from j-SR. They were arranged approximately parallel to the longitudinal axis of the myocyte and occurred at regular intervals of ~1.9 μm. In this cell, the center-to-center distance between individual sites ranged from 1.41 μm to 2.89 μm; its mean value was 1.89 ± 0.15 μm ($n = 9$).

A more detailed analysis of the two leftmost release sites marked by the red circles (Fig. 6 *Ab*) is presented in Figs. 6 *C–E*. Fig. 6 *D* (*red traces*) shows $[Ca^{2+}]_i$ transients originating from these sites at three different times: (1) during the microscopic wave shown in Fig. 6 *B*; (2) during a second microscopic wave occurring ~4 s later at the same region; and (3) during a global $[Ca^{2+}]_i$ increase presumably triggered by a spontaneous action potential. In Fig. 6 *D*, *a*, *b*, and *c* correspond to the images illustrated in Fig. 6 *C*. The two sites could be clearly identified in each of the three images (*arrowheads*) as well as in the accompanying profile plots along the dashed line (peaks marked by the *red arrows*). For comparison, the $[Ca^{2+}]_i$ signals from an area between these release sites (*blue circle* and *blue arrows* in Fig. 6, *Ab* and *C*, respectively) and from a nearby central site (*green circle* in Fig. 6 *Ab*) are also plotted in Fig. 6 *D*. The first derivative of each of these signals, i.e., the approximated Ca^{2+} release flux, is shown in Fig. 6 *E*. As expected for true Ca^{2+} release sites, the red sites exhibited the highest amplitude $[Ca^{2+}]_i$ transients and the highest Ca^{2+} fluxes, whereas the blue nonrelease site in between revealed lower amplitudes and fluxes.

In contrast to the large signals obtained from the two active release sites in the periphery, the nearby central area (*green*) did not display a significant $[Ca^{2+}]_i$ increase

FIGURE 6 during a spontaneously occurring action potential reveal that the location of the two subsarcolemmal release sites marked by the arrowheads is constant. *Right:* Accompanying fluorescence profiles along the dashed line. The red arrows mark the two release sites, whereas the blue arrow identifies a nonrelease site in the middle (see *Ab*). F/F_0 scale from 1 to 8 applies to (*c*) only. (*D*) $[Ca^{2+}]_i$ transients from two subsarcolemmal release sites (two *red traces* are largely overlapping), a nonrelease site in between (*blue*), and a nearby central site (*green*) during two microscopic $[Ca^{2+}]_i$ waves and a spontaneously occurring action potential (colors as in *Ab* and *C*). Labels *a*, *b*, and *c* refer to the images presented in (*C*). (*E*) Corresponding approximated Ca^{2+} release fluxes (normalized; colors as before).

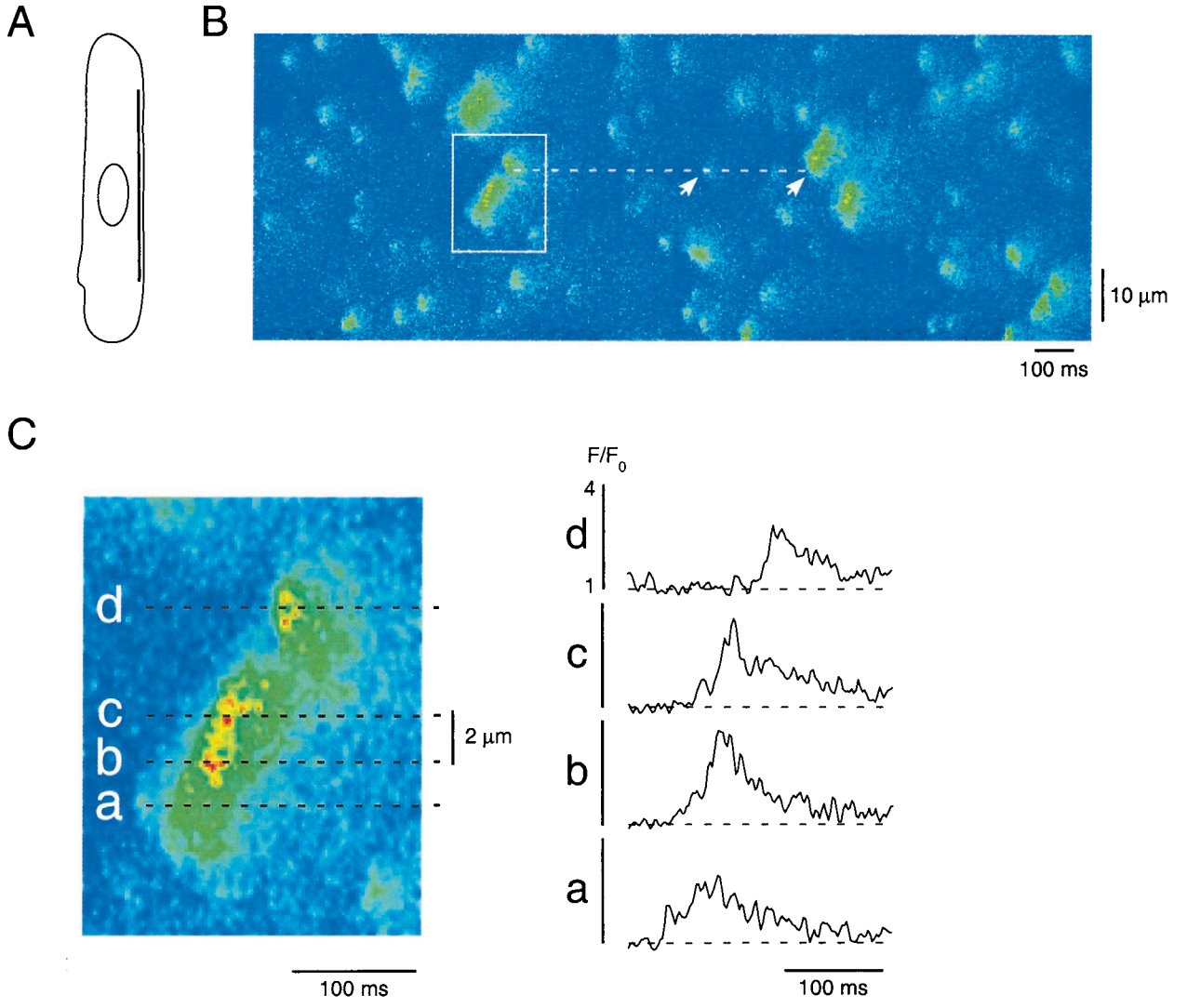

FIGURE 7 Coupled Ca^{2+} sparks as visualized by confocal linescan imaging. (*A*) The scanned line was positioned directly underneath the sarcolemma of an atrial myocyte. (*B*) Subsarcolemmal Ca^{2+} sparks and microscopic $[Ca^{2+}]_i$ waves. (*C*) Enlarged view of the microscopic wave shown in the boxed area in (*B*). Four release sites are identified along the dashed lines (*a–d*). $[Ca^{2+}]_i$ signals along the dashed lines are shown on the right. The site between (*c*) and (*d*), apparently failing during the wave, is activated later (*dashed line* and *arrows* in *B*).

during the microscopic waves. The very small central signal (*green trace* in Fig. 6 *D*) was most likely due to simple diffusion of Ca^{2+} from the region of the subsarcolemmal $[Ca^{2+}]_i$ waves, demonstrating that there was no active Ca^{2+} release from the central nj-SR under these conditions, and that the $[Ca^{2+}]_i$ waves were restricted to the subsarcolemmal space. During the action potential-induced $[Ca^{2+}]_i$ transient, however, there was a large $[Ca^{2+}]_i$ increase at the central site (Fig. 6 *Dc*). Its rising phase (Fig. 6 *D*) and peak flux (Fig. 6 *E*) were delayed compared with the subsarcolemmal sites. Furthermore, during the later part of the $[Ca^{2+}]_i$ transient, the Ca^{2+} release flux in the center was clearly larger than the already declining flux in the periphery (Fig. 6 *E*). Taken together, these results strongly suggest that there was active Ca^{2+} release from the central stores during the action potential, but not during the microscopic waves.

Microscopic $[Ca^{2+}]_i$ waves were analyzed in seven atrial cells obtained from five cat hearts. They were comprised of 2–16 individual release sites and tended to occur at the same subsarcolemmal regions within a given myocyte. Overall, the average distance between a total of 83 Ca^{2+} release sites was 1.80 ± 0.05 μm (n = 70).

Fig. 7 illustrates the appearance of a microscopic $[Ca^{2+}]_i$ wave as recorded in the linescan mode of the conventional laser scanning confocal microscope. To measure subsarcolemmal Ca^{2+} spark activity, the scan line was positioned directly under the surface membrane of a resting atrial myocyte as indicated in Fig. 7 *A*. A multitude of Ca^{2+} sparks was observed (Fig. 7 *B*), many of them occurring

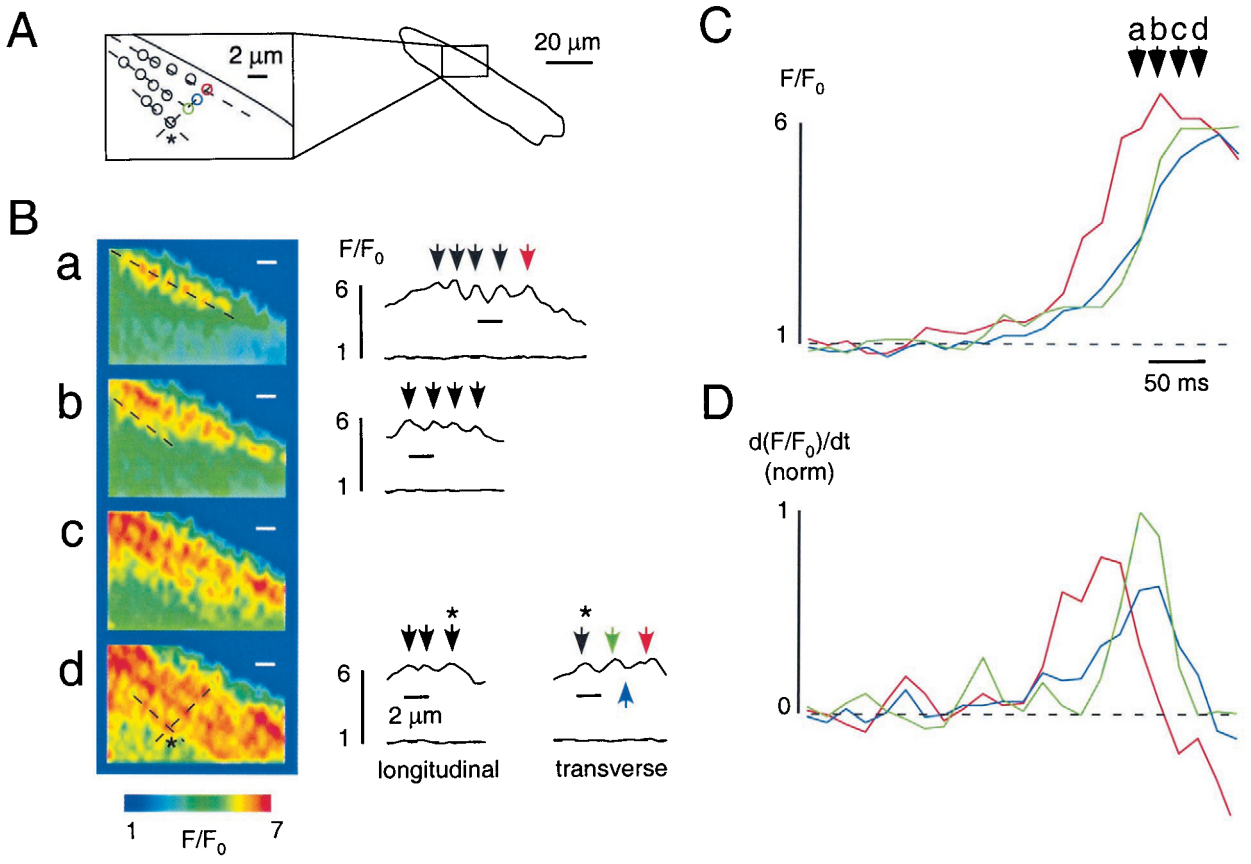

FIGURE 8 Global $[Ca^{2+}]_i$ wave revealing the arrangement of individual Ca^{2+} release sites of subsarcolemmal j-SR and central nj-SR. (*A*) Ca^{2+} release sites (*black*, *green*, and *red circles*) of a subcellular region (*boxed area*) of an atrial myocyte. A nonrelease site (*blue circle*) is also shown. Four consecutive images (*a–d*) obtained during a spontaneous $[Ca^{2+}]_i$ wave are shown in (*B*). Three longitudinal (*a–c*) and one transverse (*d*) fluorescence profiles along the dashed lines are displayed (*B*, *right*) revealing the activation of distinct Ca^{2+} release sites (*downward arrows*) of j-SR (*a*) and nj-SR (*b* and *d*). Asterisks in (*A*) and (*Bd*) indicate the innermost release site. (*C*) $[Ca^{2+}]_i$ signals from three different sites: (1) the j-SR release site marked by the red circle in (*A*) and the red arrows in (*B*); red trace, (2) the nj-SR release site marked by the green circle in (*A*) and the green arrow in (*B*); green trace, and (3) a nonrelease site found in between the former two sites (*blue circle* in *A* and *blue arrow* in *B*); blue trace. Labels *a–d* refer to the images in (*B*). (*D*) Approximated Ca^{2+} release fluxes derived from the $[Ca^{2+}]_i$ signals shown in (*C*) (normalized; colors as before).

repeatedly at the same locations. Some larger Ca^{2+} release events were also present including the microscopic $[Ca^{2+}]_i$ wave shown in more detail in Fig. 7 *C*. The wave propagated with a velocity of 86 $\mu m\ s^{-1}$ over a distance of 8 μm. Four release sites (*a–d*) were identified along the wavefront. The distance between *a* and *b* and *b* and *c* was ~1.7 μm, whereas sites *c* and *d* were separated by 4.2 μm. Apparently, a site in the middle failed during the microscopic wave but it was clearly activated later during the recording (*dashed line* and *arrows* in Fig. 7 *B*). Using both Ca^{2+} sparks and microscopic waves to determine the location of single subsarcolemmal release sites, 63 sites with a mean distance of 1.87 ± 0.07 μm ($n = 60$) were mapped in confocal linescan images obtained from three atrial myocytes. Thus, the numbers for both wave velocity and distance between individual release sites were in good agreement with the results obtained by 2-D imaging.

Activation of Ca^{2+} release sites from central stores during macroscopic $[Ca^{2+}]_i$ waves

Macroscopic (global) $[Ca^{2+}]_i$ waves were observed less frequently. They were often triggered by microscopic waves and seemed to occur only in cells that were Ca^{2+}-overloaded. Macroscopic waves, however, allowed the identification of individual Ca^{2+} release sites from central stores (nj-SR) as illustrated in Fig. 8. In this atrial myocyte (Fig. 8 *A*), a subsarcolemmal $[Ca^{2+}]_i$ wave started in the upper left region of the boxed area. The wave spread inwardly (and further along the periphery) eventually triggering an action potential. Details of the inward propagation are shown in four consecutive images (*a–d*) in Fig. 8 *B*. Distinct $[Ca^{2+}]_i$ peaks indicative of individual SR release sites were observed. They occurred in rows parallel to the longitudinal axis of the cell. Thus, during the inward propagation of the $[Ca^{2+}]_i$ wave, a grid of release sites became apparent (*d*).

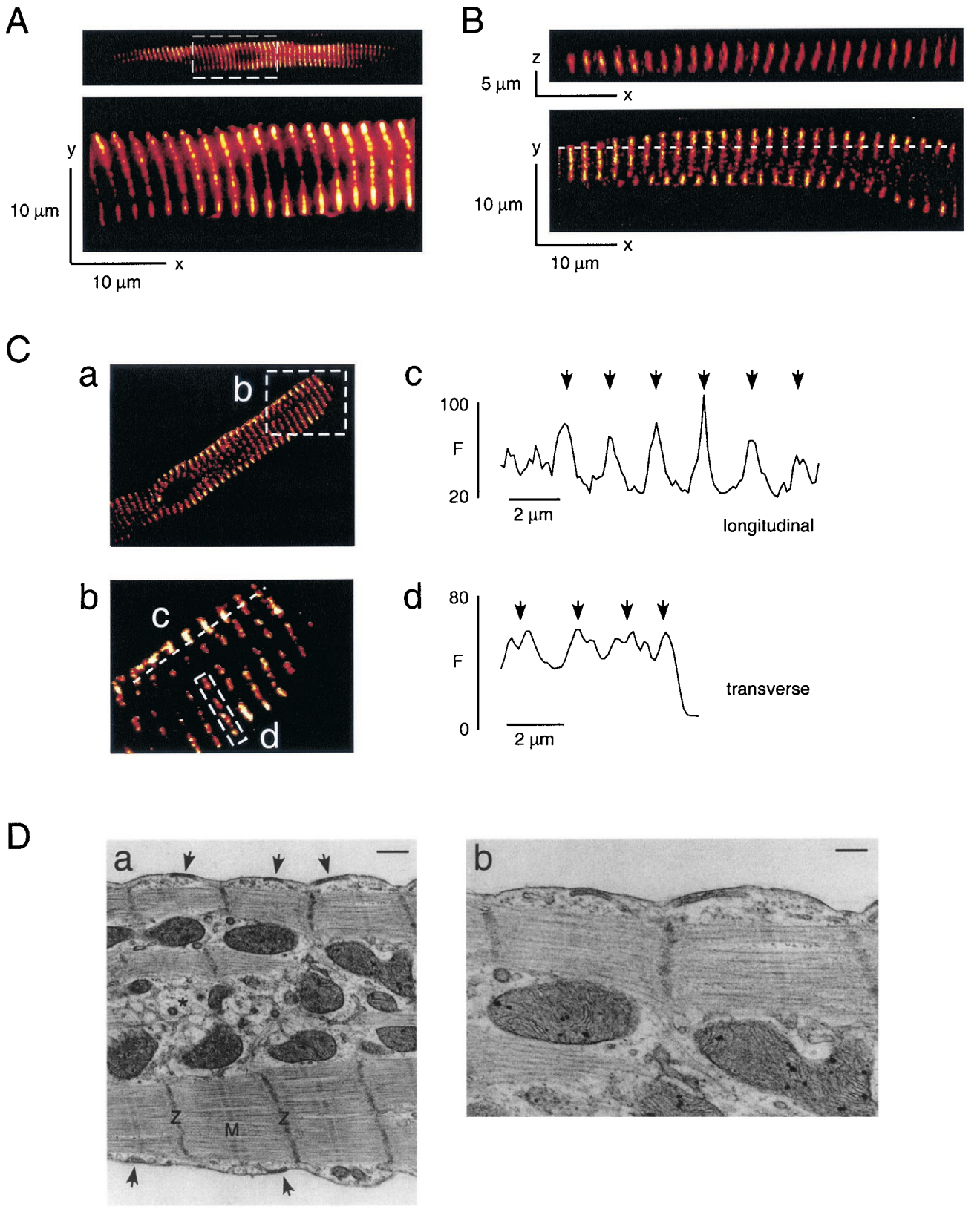

FIGURE 9 Distribution of ryanodine receptors and SR in cat atrial myocytes. (*A*) Epifluorescence images of an atrial myocyte immunostained for RyRs. Bottom image is a magnification of the boxed area. Transverse bands of RyR immunofluorescence are observed at regular intervals of ~1.9 μm. (*B*) Confocal images of a different cell. Top image is an *x–z* section (0.4 μm axial steps) along the dashed line shown in the bottom (*x–y*) image. RyR bands

The profile plots of the dashed lines in *a*, *b*, and *d* confirm the presence of the individual release sites. They are shown on the right in Fig. 8 *B*. The downward arrows indicate the respective release site. For easier identification, the innermost site is marked by the asterisk. The location of the release sites as derived from the images and the profile plots (Fig. 8 *B*) is shown in Fig. 8 *A*. In this example, 15 sites aligned in three rows could be mapped. Their distance was ~2 μm in each row. The $[Ca^{2+}]$ signals and approximated release fluxes for two of them (*red* and *green circles* and *arrows* in Fig. 8, *A* and *B*, respectively) before and during the beginning of the wave are plotted in Fig. 8, *C* and *D*. In addition, the signal of a nonrelease site in the middle (*blue circle* and *arrow* in Fig. 8, *A* and *B*) is also shown. Labels *a–d* refer to the respective images presented in Fig. 8 *B*. Clearly, the subsarcolemmal release site (*red*) was activated first. $[Ca^{2+}]_i$ then increased at the nonrelease site (*blue*) before the neighboring central site in the second row (*green*) was activated. The slow increase and the low amplitude of the $[Ca^{2+}]_i$ signal at the blue site clearly identify it as a nonrelease site, whereas the higher amplitudes and rates of rise of the red and green sites demonstrate that they are Ca^{2+} release sites from the j-SR and nj-SR, respectively.

In three atrial myocytes, release sites were mapped and analyzed from global $[Ca^{2+}]_i$ waves. Fifty-two Ca^{2+} release sites from central nj-SR compartments were identified. They occurred in two rows approximately parallel to the longitudinal axis of the cells. The distance between the two rows of nj-SR release sites varied from ~1.5 μm to 2.4 μm. Twenty-six nj-SR release sites were identified within each of these rows with a mean center-to-center distance of 1.79 ± 0.10 μm ($n = 21$) and 1.69 ± 0.05 μm ($n = 21$) for the first and second nj-SR row, respectively.

Distribution of SR Ca^{2+} release channels (RyRs) and sarcoplasmic reticulum

The distribution of RyRs within the atrial myocytes was visualized using immunocytochemistry. Initially, a group of cells was probed for α-actinin both as a control and to establish the location of the Z-lines (data not shown). Homogeneously labeled transverse bands of fluorescence were observed at a sarcomeric spacing of 1.71 ± 0.08 μm ($n = 6$ cells). The transmitted light images acquired simultaneously exhibited light and dark bands corresponding to the I- and A-bands, respectively. The light I-bands aligned with the α-actinin immunofluorescence, demonstrating that the Z-lines are located within the I-bands. Next, myocytes were probed for RyRs. Fig. 9 *A* shows a representative pattern of RyR distribution in an atrial myocyte as visualized by nonconfocal epifluorescence microscopy. Similar to α-actinin, RyR immunofluorescence formed transverse bands spaced ~2 μm apart. As was the case for α-actinin, RyR immunoreactivity coincided with the light I-bands of the transmitted light images, suggesting that RyRs were located predominantely near the Z-lines. Confocal microscopy was used to analyze the 3-D distribution of the RyRs in more detail. Fig. 9 *B* (*bottom*) shows a confocal image of an atrial myocyte taken at a central axial depth. An *x–z* scan (0.4 μm increments in axial direction) at the location of the dashed white line demonstrated that the RyR pattern was conserved through the entire depth of the cell (Fig. 9 *B*, *top*). To quantify the distance between bands of RyRs, the fluorescence profile of a selected region of the cell was plotted. The distance between individual peaks was then measured as illustrated in Fig. 9 *C*. Fig. 9 *Cb* shows an enlarged view of the boxed area of the atrial myocyte depicted in Fig. 9 *Ca*. Punctate bands of RyR immunoreactivity occurred at regular intervals. The profile plot of the dashed white line (*c*) revealed distinct fluorescence peaks spaced ~2 μm apart (Fig. 9 *Cc*, *arrows*). In a total of six myocytes, the average distance between these peaks was 1.90 ± 0.05 μm. Furthermore, a transverse plot along the RyR band shown in the small boxed area (*d*) indicated four sites of higher immunofluorescence (Fig. 9 *Cd*, *arrows*), suggesting that RyRs were clustered along the band. Limitations on substrate (RyR) accessibility to antibody seem unlikely to account for this observation, as the punctate pattern of RyR immunolocalization contrasts significantly with the complete banding pattern exhibited by α-actinin. Additionally, the localization of α-actinin (confocal reconstruction; not shown) and RyRs (Fig. 9 *B*, *top*) was continuous across the myocyte, suggesting a thorough permeabilization of the cell and extensive accessibility of antibodies to the cell interior.

Electron microscopy was used to study the distribution of j-SR and nj-SR. The electron micrograph in Fig. 9 *Da* shows a longitudinally cut section of an atrial myocyte. Sarcomeres and mitochondria were the most prominent structures inside the cell. In addition, the center of the myocyte revealed extensive nj-SR (∗) visible as a network of interconnected tubules with a diameter of ~40 nm. Furthermore, peripheral couplings (*arrows*) were present at the surface membrane. The peripheral couplings are flattened vesicles of j-SR. They were 200–400 nm wide and came into close contact (~15 nm) with the plasma membrane (Fig. 9 *Db*). Peripheral couplings were regularly distributed within the cells. With very few exceptions, each

FIGURE 9 traverse the entire depth of the myocyte. (*C*) Confocal images (*a* and *b*) and fluorescence profiles (*c* and *d*). Enlarged view (*b*) of the boxed area in (*a*) demonstrates punctate bands of RyR immunofluorescence. Longitudinal (*c*) and transverse (*d*) fluorescence profiles along the dashed line and from the boxed area reveal fluorescence peaks (*arrows*) spaced ~2 μm apart in both dimensions, suggesting that RyRs are clustered along the bands. (*D*) Electron micrographs of a longitudinally cut atrial myocyte. (*a*) SR is present as peripheral couplings of j-SR with the plasma membrane (*arrows*) and as a network of nj-SR in the cell center (∗); M, M-line; Z, Z-line. (*b*) Magnified view of two sarcomeres containing one peripheral coupling each. The left coupling is close to an M-line, whereas the right one is near a Z-line. Calibration bars, 400 nm (*a*) and 200 nm (*b*).

sarcomere contained one peripheral coupling. However, the location of a coupling within a sarcomere was variable with some occurring near an M-line whereas others were closer to a Z-line. Peripheral couplings were connected to the nj-SR (not shown), suggesting that a continuous sarcotubular network traverses the entire myocyte.

DISCUSSION

The most important finding of our study is the visualization of the propagated activation of individual j-SR and nj-SR Ca^{2+} release sites during electrically evoked $[Ca^{2+}]_i$ transients and spontaneously occurring $[Ca^{2+}]_i$ waves. Direct evidence is presented that, in atrial myocytes, both whole-cell $[Ca^{2+}]_i$ transients and $[Ca^{2+}]_i$ waves are the result of the spatial and temporal summation of individual Ca^{2+} release events from the subsarcolemmal (junctional) and central (nonjunctional) SR. Experiments were conducted at low stimulation rates and at room temperature to better resolve these events. The Ca^{2+} release sites were identified by their higher amplitude $[Ca^{2+}]_i$ transients and the higher underlying Ca^{2+} fluxes, which clearly distinguished them from neighboring nonrelease sites. Importantly, the location of the identified release sites (and nonrelease sites) was constant during repetitive activity (Figs. 2, 3, and 6). The mapping of functional release sites in combination with the immunostaining of RyRs (Fig. 9 *A–C*) and visualization of the SR by electron micoscopy (Fig. 9 *D*) indicated that RyR-Ca^{2+} release sites are organized in a regular 3-D grid. The average longitudinal and transverse distances between individual release sites in this grid was $\sim 2\ \mu m$ in both dimensions. Previous studies in human, rabbit, and rat atrium have revealed a similar sarcomeric pattern of RyR immunostaining (Hatem et al., 1997; Lewis Carl et al., 1995; Mackenzie et al., 2001). Moreover, in rat RyR fluorescence bands were also found to be punctate, suggesting that, at least in rat and cat atrium, RyRs are transversely clustered along the nj-SR.

Electrically evoked $[Ca^{2+}]_i$ transients started at distinct locations in the periphery. Release from these subsarcolemmal sites subsequently fused to form a peripheral ring of elevated $[Ca^{2+}]_i$. The magnitude of Ca^{2+} release from single sites could vary from beat to beat. Also, the activation order of individual sites varied significantly during consecutive stimulations (Fig. 3), suggesting that Ca^{2+} release from these sites was triggered during the action potential by stochastic openings of sarcolemmal DHPRs known to colocalize with RyRs in the j-SR membrane (Lewis Carl et al., 1995). Interestingly, the opposite seems to be true for rat atrial myocytes (Mackenzie et al., 2001) and skeletal muscle (Blatter et al., 1996). In these preparations some "eager" release sites responded in a reproducible fashion to repetitive depolarizations. In rat atrial myocytes the eager sites were the first to show a $[Ca^{2+}]_i$ increase upon stimulation and had the highest frequencies of spontaneous Ca^{2+} sparks. Based on these observations the authors speculated that the strict activation sequence of the subsarcolemmal "eager" release sites may be attributable to a higher intrinsic Ca^{2+} sensitivity of those sites and a close coupling to adjacent DHPRs (Mackenzie et al., 2001).

Our results demonstrate that the subsarcolemmal Ca^{2+} release sites are functionally coupled. In terms of E-C coupling, this property, in combination with Ca^{2+} influx through voltage-dependent L-type channels, translates into a reliable subsarcolemmal build-up of elevated $[Ca^{2+}]_i$ at the beginning of the action potential-induced $[Ca^{2+}]_i$ transient, visualized as a ring of elevated $[Ca^{2+}]_i$ in 2-D confocal images. The subsarcolemmal elevation of $[Ca^{2+}]_i$, in turn, is crucial for the inward propagation of the $[Ca^{2+}]_i$ transient by CICR and contraction of the myocyte. Ca^{2+} release from the central nj-SR was somewhat smaller than from the subsarcolemmal j-SR. In the center of the cell, $[Ca^{2+}]_i$ transient amplitude reached, on average, only $\sim$75% of the amplitude recorded in the subsarcolemmal space (although in some cells, central release slightly exceeded peripheral release). Nevertheless, significant Ca^{2+} release from the nj-SR, triggered by propagating CICR from the j-SR, was clearly present (Figs. 4 and 5). The robust Ca^{2+} release from central SR compartments observed in cat and guinea-pig atrial myocytes (Berlin, 1995; Hüser et al., 1996, 2000) is at variance with two recent studies indicating that, at least under basal conditions, rat atrial myocytes and rabbit cardiac Purkinje cells (which share a similar ultrastructure with atrial myocytes, including the presence of central RyRs and the absence of T-tubules) do not exhibit significant Ca^{2+} release from the central nj-SR (Cordeiro et al., 2001; Mackenzie et al., 2001). The reason for this discrepancy remains unclear. It seems plausible, however, that the lack of CICR from central SR compartments observed in the Purkinje myocytes may be because of the comparatively low subsarcolemmal $[Ca^{2+}]_i$ which typically does not exceed 500 nM in these cells (Cordeiro et al., 2001). Activation of RyRs, however, is thought to require local $[Ca^{2+}]_i$ in the micromolar range. Thus, local $[Ca^{2+}]_i$ in the Purkinje myocytes may not be sufficiently high to activate nonjunctional RyRs in the center of the cells, whereas in the cat atrial myocytes, because of the large subsarcolemmal $[Ca^{2+}]_i$ increase, these requirements may be fulfilled.

The observation of subsarcolemmal microscopic $[Ca^{2+}]_i$ waves and coupled Ca^{2+} sparks has important ramifications for the understanding of atrial E-C coupling. Microscopic $[Ca^{2+}]_i$ waves were regularly seen in unstimulated myocytes. They occurred in the subsarcolemmal space but not in central regions of the cell, suggesting that there is a preferential coupling of neighboring subsarcolemmal Ca^{2+} release sites. Considering that the distance between a particular subsarcolemmal release site and its nearest subsarcolemmal or central neighbor is similar ($\sim 2\ \mu m$), one would assume, to a first approximation, that the diffusional

distance for Ca^{2+} is similar in both directions and that Ca^{2+} release would propagate via CICR in both directions with similar likelihood. The observation of preferential subsarcolemmal propagation of sparks and waves is inconsistent with this prediction. Several possibilities could account for this observation. J-SR and surface membranes in atrial myocytes form peripheral couplings (Fig. 9 *D*) which are reminiscent and functionally homologous to dyads and triads in T-tubule-containing cells (McNutt and Fawcett, 1969; Sommer and Jennings, 1992). This structural arrangement of the j-SR raises the possibility that the local $[Ca^{2+}]_i$ in this cleft might be higher than in the vicinity of nj-SR Ca^{2+} release sites and, therefore, the local diffusional gradient for Ca^{2+} might be higher. Furthermore, the specific arrangements of j-SR and surface membranes may actually favor restricted lateral diffusion of Ca^{2+} and thereby facilitate subsarcolemmal propagation of Ca^{2+} sparks. Alternative or additional explanations, which are not mutually exclusive, are the possibilities that subsarcolemmal release sites exhibit a higher $[Ca^{2+}]_i$ sensitivity than their central counterparts, that the number or the density of RyRs is higher in the j-SR, and/or that there are differences in Ca^{2+} load between j-SR and nj-SR. A higher Ca^{2+} load of the j-SR could enhance subsarcolemmal SR Ca^{2+} release via the known sensitivity of the RyR to intraluminal free $[Ca^{2+}]$ which sensitizes RyRs to cytoplasmic $[Ca^{2+}]$ and CICR (Györke and Györke, 1998). All these possibilities are consistent with the observations (1) that subsarcolemmal $[Ca^{2+}]_i$ transients are typically larger than $[Ca^{2+}]_i$ transients from central regions of the cell (Fig. 4); (2) that spontaneous Ca^{2+} sparks occur at a higher frequency in the subsarcolemmal space as compared with more central regions (Hüser et al., 1996); and (3) that Ca^{2+} sparks recorded from the subsarcolemmal space tend to have larger amplitudes (Sheehan and Blatter, 2001). For cardiac cells which lack a T-tubular system (atrial myocytes, pacemaker cells, and Purkinje cells), a preferential activation of subsarcolemmal Ca^{2+} release at the very beginning of the action potential-induced $[Ca^{2+}]_i$ transient represents a safety mechanism for subsequent activation of nj-SR release sites. By activating a large number of subsarcolemmal Ca^{2+} release sites simultaneously and rapidly, a robust centripetal $[Ca^{2+}]_i$ gradient is generated which guarantees propagation of Ca^{2+} release by CICR. Without the initial high subsarcolemmal $[Ca^{2+}]_i$ gradient, $[Ca^{2+}]_i$ near central nj-SR release sites may never reach high enough levels capable of inducing CICR. As a consequence, propagation of Ca^{2+} release may die off and remain incomplete in central regions of the myocyte as observed during the small amplitude $[Ca^{2+}]_i$ transient in cardiac electromechanical alternans (Hüser et al., 2000).

In summary, our results provide direct evidence that the spatial and temporal summation of Ca^{2+} release from individual j-SR and nj-SR release sites, organized in a 3-D grid of clustered RyRs, underlies atrial E-C coupling. The sequential activation of j-SR release sites, followed by centripetally propagating CICR from nj-SR release sites results in the characteristic inhomogeneous pattern of the action potential-induced atrial $[Ca^{2+}]_i$ transient.

This work was supported by grants from the National Institutes of Health (HL51941 and HL62231 to L.A.B., MH53367 and HL58851 to G.A.M., and HL27652 and HL63753 to S.L.L.), the AHA (95002520 to L.A.B.), and postdoctoral fellowships from the Falk Foundation (Loyola University Chicago) and the Deutsche Forschungsgemeinschaft (DFG) to J.K. K.A.S. was supported by an Arthur J. Schmitt Dissertation Fellowship (Loyola University Chicago) and a Lilly Graduate Student Fellowship in Cardiovascular Research (Loyola University Chicago and Eli Lilly and Company, Indianapolis, IN). The expert technical assistance of Holly Gray and Linda Fox is gratefully acknowledged.

REFERENCES

Berlin, J. R. 1995. Spatiotemporal changes of Ca^{2+} during electrically evoked contractions in atrial and ventricular cells. *Am. J. Physiol.* 269:H1165–H1170.

Blatter, L. A., J. Hüser, and E. Rios. 1997. Sarcoplasmic reticulum Ca^{2+} release flux underlying Ca^{2+} sparks in cardiac muscle. *Proc. Natl. Acad. Sci. U.S.A.* 94:4176–4181.

Blatter, L. A., A. Tsugorka, N. Shirokova, and E. Rios. 1996. Eager triads in skeletal muscle: heterogeneous distribution of voltage-elicited Ca^{2+} release revealed by confocal microscopy. *Biophys. J.* 70:A235.

Cannell, M. B., H. Cheng, and W. J. Lederer. 1994. Spatial non-uniformities in $[Ca^{2+}]_i$ during excitation-contraction coupling in cardiac myocytes. *Biophys. J.* 67:1942–1956.

Cheng, H., M. B. Cannell, and W. J. Lederer. 1994. Propagation of excitation-contraction coupling into ventricular myocytes. *Pflügers Arch.* 428:415–417.

Cheng, H., M. R. Lederer, R. P. Xiao, A. M. Gomez, Y. Y. Zhou, B. Ziman, H. Spurgeon, E. G. Lakatta, and W. J. Lederer. 1996. Excitation-contraction coupling in heart: new insights from Ca^{2+} sparks. *Cell Calcium.* 20:129–140.

Cheng, H., W. J. Lederer, and M. B. Cannell. 1993. Calcium sparks: elementary events underlying excitation-contraction coupling in heart muscle. *Science.* 262:740–744.

Cleemann, L., W. Wang, and M. Morad. 1998. Two-dimensional confocal images of organization, density, and gating of focal Ca^{2+} release sites in rat cardiac myocytes. *Proc. Natl. Acad. Sci. U.S.A.* 95:10984–10989.

Cordeiro, J. M., K. W. Spitzer, W. R. Giles, P. E. Ershler, M. B. Cannell, and J. H. B. Bridge. 2001. Location of the initiation site of calcium transients and sparks in rabbit heart Purkinje cells. *J. Physiol.* 531: 301–314.

Genka, C., H. Ishida, K. Ichimori, Y. Hirota, T. Tanaami, and H. Nakazawa. 1999. Visualization of biphasic Ca^{2+} diffusion from cytosol to nucleus in contracting adult rat cardiac myocytes with an ultra-fast confocal imaging system. *Cell Calcium.* 25:199–208.

Györke, I., and S. Györke. 1998. Regulation of the cardiac ryanodine receptor channel by luminal Ca^{2+} involves luminal Ca^{2+} sensing sites. *Biophys. J.* 75:2801–2810.

Hatem, S. N., A. Benardeau, C. Rucker-Martin, I. Marty, P. de Chamisso, M. Villaz, and J. J. Mercadier. 1997. Different compartments of sarcoplasmic reticulum participate in the excitation-contraction coupling process in human atrial myocytes. *Circ. Res.* 80:345–353.

Hüser, J., S. L. Lipsius, and L. A. Blatter. 1996. Calcium gradients during excitation-contraction coupling in cat atrial myocytes. *J. Physiol.* 494: 641–651.

Hüser, J., Y. G. Wang, K. A. Sheehan, F. Cifuentes, S. L. Lipsius, and L. A. Blatter. 2000. Functional coupling between glycolysis and excitation-contraction coupling underlies alternans in cat heart cells. *J. Physiol.* 524:795–806.

Lewis Carl, S., K. Felix, A. H. Caswell, N. R. Brandt, W. J. Ball, Jr., P. L. Vaghy, G. Meissner, and D. G. Ferguson. 1995. Immunolocalization of sarcolemmal dihydropyridine receptor and sarcoplasmic reticular triadin and ryanodine receptor in rabbit ventricle and atrium. *J. Cell Biol.* 129:673–682.

Lipp, P., J. Hüser, L. Pott, and E. Niggli. 1996. Spatially non-uniform Ca^{2+} signals by reduction of transverse tubules in citrate-loaded guinea-pig ventricular myocytes in culture. *J. Physiol.* 497:589–597.

Lipp, P., L. Pott, G. Callewaert, and E. Carmeliet. 1990. Simultaneous recording of indo-1 fluorescence and Na^+/Ca^{2+} exchange current reveals two components of Ca^{2+} release from sarcoplasmic reticulum of cardiac atrial myocytes. *FEBS Letters* 275:181–184.

Lopez-Lopez, J. R., P. S. Shacklock, C. W. Balke, and W. G. Wier. 1994. Local, stochastic release of Ca^{2+} in voltage-clamped rat heart cells: visualization with confocal microscopy. *J. Physiol.* 480:21–29.

Mackenzie, L., M. D. Bootman, M. J. Berridge, and P. Lipp. 2001. Predetermined recruitment of calcium release sites underlies excitation-contraction coupling in rat atrial myocytes. *J. Physiol.* 530:417–429.

McNutt, N. S., and D. W. Fawcett. 1969. The ultrastructure of the cat myocardium. II. Atrial muscle. *J. Cell Biol.* 42:46–67.

Niggli, E. 1999. Localized intracellular calcium signaling in muscle: calcium sparks and calcium quarks. *Annu. Rev. Physiol.* 61:311–335.

Pott, L., P. Lipp, G. Callewaert, and E. Carmeliet. 1991. Spatial properties of Ca^{2+} transients in cardiac myocytes studied by simultaneous measurement of Na^+-Ca^{2+} exchange current and indo-1 fluorescence. *Ann. NY Acad. Sci.* 639:354–365.

Reynolds, E. S. 1963. The use of lead citrate at high pH as an electron-opaque stain in electron microscopy. *J. Cell Biol.* 17:208–212.

Santana, L. F., H. Cheng, A. M. Gomez, M. B. Cannell, and W. J. Lederer. 1996. Relation between the sarcolemmal Ca^{2+} current and Ca^{2+} sparks and local control theories for cardiac excitation-contraction coupling. *Circ. Res.* 78:166–171.

Scriven, D. R., P. Dan, and E. D. Moore. 2000. Distribution of proteins implicated in excitation-contraction coupling in rat ventricular myocytes. *Biophys. J.* 79:2682–2691.

Shacklock, P. S., W. G. Wier, and C. W. Balke. 1995. Local Ca^{2+} transients (Ca^{2+} sparks) originate at transverse tubules in rat heart cells. *J. Physiol.* 487:601–608.

Sheehan, K. A., and L. A. Blatter. 2001. Inhomogeneity of spontaneous Ca^{2+} sparks in cat atrial myocytes. *Biophys. J.* 80:63A.

Sipido, K. R., and W. G. Wier. 1991. Flux of Ca^{2+} across the sarcoplasmic reticulum of guinea-pig cardiac cells during excitation-contraction coupling. *J. Physiol.* 435:605–630.

Soeller, C., and M. B. Cannell. 1999. Examination of the transverse tubular system in living cardiac rat myocytes by 2-photon microscopy and digital image-processing techniques. *Circ. Res.* 84:266–275.

Sommer, J. R., and R. B. Jennings. 1992. Ultrastructure of cardiac muscle. *In* The heart and cardiovascular system. H.A. Fozzard, E. Haber, R.B. Jennings, A, M, Katz, and H.E. Morgan, editors. Raven Press, New York. 3–50.

Song, L. S., J. S. Sham, M. D. Stern, E. G. Lakatta, and H. Cheng. 1998. Direct measurement of SR release flux by tracking "Ca^{2+} spikes" in rat cardiac myocytes. *J. Physiol.* 512:677–691.

Tanaka, H., T. Sekine, T. Kawanishi, R. Nakamura, and K. Shigenobu. 1998. Intrasarcomere [Ca^{2+}] gradients and their spatio-temporal relation to Ca^{2+} sparks in rat cardiomyocytes. *J. Physiol. (Lond.).* 508:145–152.

Wier, W. G., and C. W. Balke. 1999. Ca^{2+} release mechanisms, Ca^{2+} sparks, and local control of excitation-contraction coupling in normal heart muscle. *Circ. Res.* 85:770–776.

Wu, J., J. Vereecke, E. Carmeliet, and S. L. Lipsius. 1991. Ionic currents activated during hyperpolarization of single right atrial myocytes from cat heart. *Circ. Res.* 68:1059–1069.